Journal of Power Sources 196 (2011) 9284–9289

Contents lists available at ScienceDirect

Journal of Power Sources

journal homepage: www.elsevier.com/locate/jpowsour

Manganese dioxide-coated carbon nanotubes as an improved cathodic catalyst for oxygen reduction in a microbial fuel cell

Yaping Zhang[a,b,1], Yongyou Hu[a,b,*], Sizhe Li[a,b,2], Jian Sun[a,b,3], Bin Hou[a,b,4]

[a] The Key Laboratory of Pollution Control and Ecosystem Restoration in Industry Clusters, Ministry of Education, School of Environmental Science and Engineering, South China University of Technology, Guangzhou 510006, China
[b] State Key Lab of Pulp and Paper Engineering, South China University of Technology, Guangzhou 510640, China

ARTICLE INFO

Article history:
Received 19 May 2011
Accepted 20 July 2011
Available online 29 July 2011

Keywords:
Microbial fuel cell
Carbon nanotubes
Manganese dioxide
Oxygen reduction

ABSTRACT

To develop an efficient and cost-effective cathodic electrocatalyst for microbial fuel cells (MFCs), carbon nanotubes (CNTs) coated with manganese dioxide using an in situ hydrothermal method (in situ MnO_2/CNTs) have been investigated for electrochemical oxygen reduction reaction (ORR). Examination by transmission electron microscopy shows that MnO_2 is sufficiently and uniformly dispersed over the surfaces of the CNTs. Using linear sweep voltammetry, we determine that the in situ MnO_2/CNTs are a better catalyst for the ORR than CNTs that are simply mechanically mixed with MnO_2 powder, suggesting that the surface coating of MnO_2 onto CNTs enhances their catalytic activity. Additionally, a maximum power density of 210 mW m^{-2} produced from the MFC with in situ MnO_2/CNTs cathode is 2.3 times of that produced from the MFC using mechanically mixed MnO_2/CNTs (93 mW m^{-2}), and comparable to that of the MFC with a conventional Pt/C cathode (229 mW m^{-2}). Electrochemical impedance spectroscopy analysis indicates that the uniform surface dispersion of MnO_2 on the CNTs enhanced electron transfer of the ORR, resulting in higher MFC power output. The results of this study demonstrate that CNTs are an ideal catalyst support for MnO_2 and that in situ MnO_2/CNTs offer a good alternative to Pt/C for practical MFC applications.

1. Introduction

Microbial fuel cell (MFC) is a promising biotechnology that utilizes microorganisms as catalysts to decompose organic or inorganic matter and simultaneously harvest electricity [1,2]. Among many kinds of cathodic electron acceptors that can be used in an MFC, oxygen is the most suitable electron acceptor due to its limitless availability and high redox potential. However, due to the sluggish kinetics of the oxygen reduction reaction (ORR) in a medium at a pH near neutral, the power density produced by an MFC is mainly limited by the cathode performance [3,4]. Although platinum (Pt) has been widely used to enhance the ORR in MFCs, its relatively high cost limits its practical application [5]. Moreover, owing to its sensitivity to poisoning, the performance of a Pt cathode may be substantially diminished in the presence of a variety of chemicals found in wastewater [6].

To lower the cost of cathodes and simultaneously improve ORR kinetics, various non-noble metals have been investigated as cathodic catalysts for MFCs. Metal oxide catalysts such as lead dioxide [7], metal porphyrins [8], and iron phthalocyanine [9–12] have been evaluated for their ORR activity in MFC cathodes and exhibited comparable or higher performance than Pt cathodes. Recently, Co/Fe/N/CNT [13], iron-chelated ethylenediaminetetraacetic acid [14], Prussian Blue/polyaniline [15], and Co-naphthalocyanine [16] have also been proposed as alternative low-cost catalysts for MFCs. Unfortunately, the long-term instability of the transition metal macrocycles and phthalocyanines limits the practical application of these alternative catalysts [17].

Manganese oxides (MnO_x) have been widely investigated as one of the most promising catalysts for ORR in an alkaline medium [18,19]; their main advantages are their low cost and toxicity, environmental friendliness, and high chemical stability and catalytic activity. MnO_x have also been found to be promising ORR catalysts in neutral pH medium [20,21]. To date, only a few studies applying MnO_x in MFCs have been reported. Zhang et al. demonstrated that β-MnO_2/graphite was the most effective catalyst among three MnO_2 materials tested (α-MnO_2, β-MnO_2, and γ-MnO_2) due to

* Corresponding author at: School of Environmental Science and Engineering, South China University of Technology, Guangzhou 510006, China.
Tel.: +86 20 39380506; fax: +86 20 39380508.
E-mail addresses: zhang.yp@mail.scut.edu.cn (Y. Zhang), ppyyhu@scut.edu.cn (Y. Hu), lsm8611@126.com (S. Li), sunjian472@163.com (J. Sun), houbin566@163.com (B. Hou).
[1] Tel.: +86 15920480187.
[2] Tel.: +86 15989036737.
[3] Tel.: +86 20 39383779.
[4] Tel.: +86 15914305840.

0378-7753/$ – see front matter © 2011 Elsevier B.V. All rights reserved.
doi:10.1016/j.jpowsour.2011.07.069

its highest Brunauer–Emmett–Teller surface area and average oxidation states [22]. Roche et al. employed MnO_x supported on Monarch 1000 carbon black (Cabot) as the cathode catalyst and obtained a maximum power density of 161 mW m^{-2} [23]. Recently, Li et al. used carbon black powder (Cabot Vulcan XC-72) to supported MnO_x doped with cobalt, copper, and cerium to improve its catalytic performance and found that both power generation and contaminant removal were enhanced [24]. With no catalyst support material, Liu et al. demonstrated that a nano-structured MnO_x prepared by an electrochemical deposition method was an effective ORR catalyst in an MFC, generating a peak electrical power density of 772.8 mW m^{-3} [25]. However, it is known that the structure of supporting material for the active site significantly affects ORR performance as well as the metal catalyst [26,27]. Catalyst support materials such as Vulcan XC-72, Black Pearl, and Monarch 1000 carbon black, graphite, and other carbon materials are commonly used, but these supports are known to be weakly active for the ORR. In addition, due to the dense morphology and the intrinsically poor electrical conductivity of MnO_x, its electrochemical alone performance is unsatisfactory [28]. Hence, to improve the ORR performance of MnO_x and the runtime duration of a fuel cell, MnO_x can be incorporated into the electron-conductive materials. Due to their outstanding physical properties (such as high chemical stability, high aspect ratio, strong mechanical strength, nanosize morphology, and high activated surface area), carbon nanotubes (CNTs) have been demonstrated to be advantageous as catalyst support material by improving catalyst dispersion [29–31]. Thus, MnO_x/CNTs nanocomposites have been explored in attempts to improve electrochemical catalyst performance. For instance, MnO_x/CNTs nanocomposites have been shown to exhibit good ORR activity and to orientate the ORR mechanism toward the four-electron pathway in an alkaline medium [18]; and they have also been demonstrated to have excellent ractivity in lithium batteries [32]. However, to our knowledge, there have been no previous reports on the study of MnO_x/CNTs as an ORR catalyst for MFCs. Thus, there is a need to study the ORR properties of MnO_x/CNTs in a neutral-pH medium. In addition, an elucidation of MnO_x/CNTs in enhancing cathodic oxygen reduction in an MFC is interesting.

This study proceeded in three phases, as follows (i) the synthesis of MnO_2/CNTs hybrid nanostructures by a simple in situ hydrothermal method (ii) catalyst characterization using transmission electron microscopy (TEM) and X-ray diffraction (XRD) and (iii) evaluation on the ORR activity of the MnO_2/CNTs hybrid nanostructures using linear sweep voltammetry (LSV) and performance examination in a batch single-chamber MFC.

2. Experimental

2.1. Catalyst preparation

The MnO_2/CNTs hybrids were synthesized by a simple in situ hydrothermal method [33]. Specifically, 0.5 g of dodecyl benzene sulfonic acid sodium (SDBS, $C_{18}H_{29}SO_3Na$) and 0.075 g of CNTs (diameter of 20–40 nm in diameter, Shenzhen Nanotech Port Co., Ltd.) were added to 40 ml of mixture containing 0.005 M $MnSO_4{\cdot}H_2O$ and 0.005 M $KMnO_4$. After stirring for 2 h, the mixture was loaded into a Teflon-lined stainless-steel autoclave. The autoclave was heated to 160 °C and kept at 160 °C for 12 h and was then cooled naturally to room temperature. The black precipitate was separated by centrifugation and washed three times with ethanol. The product was then vacuum-dried at 60 °C overnight. Based on a mass balance calculation, 30% of the MnO_2 was incorporated into the MnO_2/CNTs composite. For comparison, α-MnO_2 was synthesized by a hydrothermal method, as previously described [34].

2.2. Electrode preparation

Air cathodes were made of carbon paper with a projected surface area of 7 cm^2. The waterproof layer was first produced as described by Cheng et al. [3]. The catalytic layer was then prepared as follows. Twenty-one milligrams of the MnO_2/CNTs hybrid and 150 μL of a 5 wt.% Nafion solution in N-methyl-2-pyrrolidone were mixed in a plastic container and then ground sufficiently to ensure good dispersion. Subsequently, the suspension was coated onto the surface of the carbon paper and was air-dried overnight and then dried under vacuum at 80 °C for 24 h to remove the solvent. The MnO_2/CNTs hybrid-modified carbon paper was designated as the "in situ MnO_2/CNTs" catbode. For comparison, α-MnO_2 powder (30 wt.%) was mechanically mixed with CNTs (70 wt.%) in a plastic container and the same procedure was followed to make cathodes (designated as the mechanically mixed MnO_2/CNTs). As controls, the Pt and bare CNTs-modified carbon paper were fabricated using the same procedure. The MnO_2 and Pt catalysts were both loaded onto the carbon paper cathodes at 1 ± 0.1 mg cm^{-2}. Using the same method, a catalyst-modified glassy carbon (GC) disk (3 mm in diameter) was prepared with a catalyst loading of 0.5 mg cm^{-2} for use in the linear sweep voltammetry (LSV) trials.

2.3. MFC setup and operation

An air-cathode single-chamber MFC was constructed as previously described [35] but a different volume. The total volume of the MFC was enlarged to 58 mL; the anode chamber was 3 cm long and 5 cm in diameter. The cathode was placed on one side of the MFC, with the oxygen catalyst coating layer facing the anode. An ultrafiltration membrane with a molecular cutoff weight of 1 kD was applied directly onto the water-facing side of the cathode. Graphite felt with a projected surface area of 7 cm^2, was used as an anode without further treatment and was positioned in the chamber at a distance of 1 cm from the cathode. MFC reactors were inoculated using anaerobic sludge collected from the Liede municipal wastewater treatment plant, Guangzhou, China. All reactors were fed with a medium containing glucose (500 mg L^{-1}), a phosphate buffer solution (PBS, 50 mM), minerals (12.5 mL L^{-1}), and vitamin solution (12.5 mL L^{-1}) [36]. The anode solution was refreshed when the voltage decreased to below 20 mV, and the suspended biomass was reserved, forming a fed-batch. All experiments were conducted in a temperature-controlled room at 30 ± 1 °C in duplicate, and the average values are reported.

2.4. Analysis and calculation

The voltage across a 500 Ω external resistor was recorded every 11 min with a multimeter and a data acquisition system (Model 2700, Keithly Instruments, USA). Polarization curves were obtained by varying the external resistance (R_{ex}) over a range from 50 to 8,000 Ω when the voltage output approached a steady and repeatable state. Current density (Am^{-2}) was calculated as $I = U/(R_{ex}S)$, and power density (mW m^{-2}) was calculated according to $P = 1000$ UI/A, where I (A) is the current, U (V) is the voltage, and A (m^2) is the projected surface area of the cathode.

To characterize the crystal structure of the catalysts, X-ray diffraction (XRD) analysis was conducted using an X-ray diffractometer (Bruker D8 Advance, Germany) equipped with a Cu Kα radiation source at a power of 40 kV × 40 mA. All patterns were obtained in the range of 10–70° (2θ), and the scanning rate was set at 0.02° step^{-1} or 17.7 s step^{-1}. The morphology and size of the catalyst samples were observed with a transmission electron microscope (TEM, JEM-1010, Hitachi) with an accelerating voltage of 100 kV. The freshly prepared catalyst samples were dispersed by ultrasonication before testing.

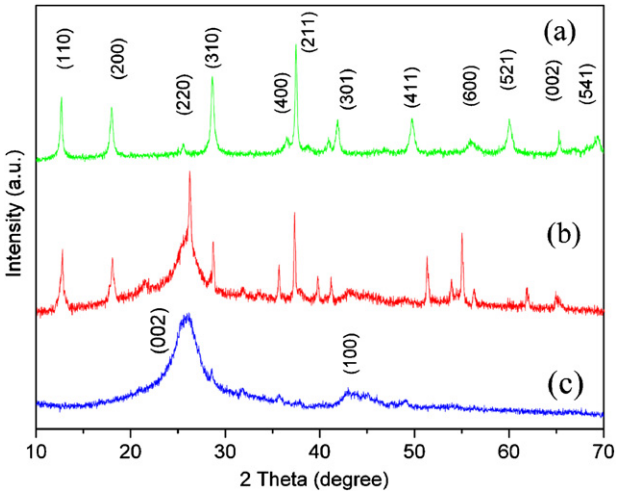

Fig. 1. XRD of (a) MnO_2 nanorods, (b) in situ MnO_2/CNTs hybrid and (c) bare CNTs.

LSV and electrochemical impedance spectroscopy (EIS) were used to electrochemically characterize the catalyst using a potentiostat (Model 2273, Princeton Applied Research) with a three-electrode setup consisting of a working electrode (the catalyst-modified GC and a cathode for LSV and EIS, respectively), an Ag/AgCl (saturated KCl) reference electrode, and a platinum foil counterelectrode. LSV was performed between 0.25 V and −0.80 V in a 50 mM PBS electrolyte. EIS tests were conducted in the MFC under open-circuit voltage (OCV) conditions over a frequency range of 10 kHz to 5 mHz, with a sinusoidal perturbation of amplitude 10 mV.

3. Results and discussion

3.1. Characteristics of the MnO_2/CNTs hybrid

Fig. 1a presents the XRD patterns of the as-prepared MnO_2 sample (without added CNTs), showing thirteen main peaks of (1 1 0), (2 0 0), (2 2 0), (3 1 0), (4 0 0), (2 1 1), (3 0 1), (4 1 1), (6 0 0), (5 2 1), (0 0 2) and (5 0 1), confirming the formation of pure α-MnO_2 crystals based on comparison with JCPDS No. 44-0141. Fig. 1c shows the XRD patterns of the CNTs, the diffraction peaks at the 2θ values of 26° and 42° were ascribed to the (0 0 2) and (1 0 0) reflections, respectively of the CNTs. [37]. Fig. 1b shows the XRD patterns of the MnO_2/CNTs hybrid. Apart from the characteristic the CNTs (0 0 2) and (1 0 0) peaks, all the other peaks could be indexed to the tetragonal phase of α-MnO_2 (JCPDS No. 44-0141), indicating that α-MnO_2 had been incorporated into the MnO_2/CNTs hybrid sample.

TEM was further performed to characterize the microstructures of the samples. As shown in Fig. 2A, the pure CNTs had a hollow-centered structure with outside diameters ranging from 20 to 40 nm and inside diameters less than 10 nm. It is clear that the pure MnO_2 was composed of rod-like or needle-like crystallites with diameters less than 20 nm and lengths ranging from tens to hundreds of nanometers, and there were many occurrences of aggregations (Fig. 2B). As shown in Fig. 2C, we observed that the MnO_2 in the mechanically mixed MnO_2/CNTs formed large aggregates that were easily detached from the CNTs. Fig. 2D shows the morphology and microstructure of the in situ MnO_2/CNTs hybrid in detail; here, there is no sign of MnO_2 aggregates. On the contrary, MnO_2 is uniformly distributed over the surface of the CNTs. Evidently, the hydrothermally coated MnO_2 had a strong interaction with the CNTs (Fig. 2D) than the MnO_2 that was mechanically mixed with the CNTs (Fig. 2C). Additionally, the coated MnO_2 could not be removed even under intensive sonication, indicating that the interaction between the MnO_2 and the CNTs is very stable. The MnO_2 crystals were noticeably intertwined with the highly conductive CNTs, thus forming a three-dimensional network structure. This three-dimensional nanostructure was expected to provide a large reaction interface, which can facilitate efficient electron transport [33]. Therefore, these features of the in situ MnO_2/CNTs hybrid make it well suited as an ORR catalyst in neutral medium.

3.2. Electrochemical activity of the MnO_2/CNTs hybrid in the ORR

Linear sweep voltammetry (LSV) of various catalysts was conducted in 50 mM PBS medium (pH = 7) saturated with N_2 or O_2. As shown in Fig. 3A, the voltammetric response of the bare CNTs was flat in the N_2-saturated solution (line a′) and yielded a small ORR peak at −0.41 V in the O_2-saturated solution (line a). Distinctive reduction peaks were observed with both MnO_2-based electrodes in the N_2-saturated solution, likely due to proton insertion process running according to the following reaction:

$$MnO_2 + H_2O + e^- \rightarrow MnOOH + OH^-$$

Fig. 3 also shows that the peak current in the O_2-saturated solution (lines b and c) was more intensive than that in the N_2-saturated solution (line b′ and c′), indicating that MnO_2 can catalyze the ORR. Specially, the in situ MnO_2/CNTs had the highest catalytic activity toward the ORR because they showed a more positive peak potential (−0.18 V, line c), than either the mechanically mixed MnO_2/CNTs (−0.39 V, line b) or the bare CNTs (−0.41 V, line a). Moreover, the peak current of the in situ MnO_2/CNTs (−0.40 mA)

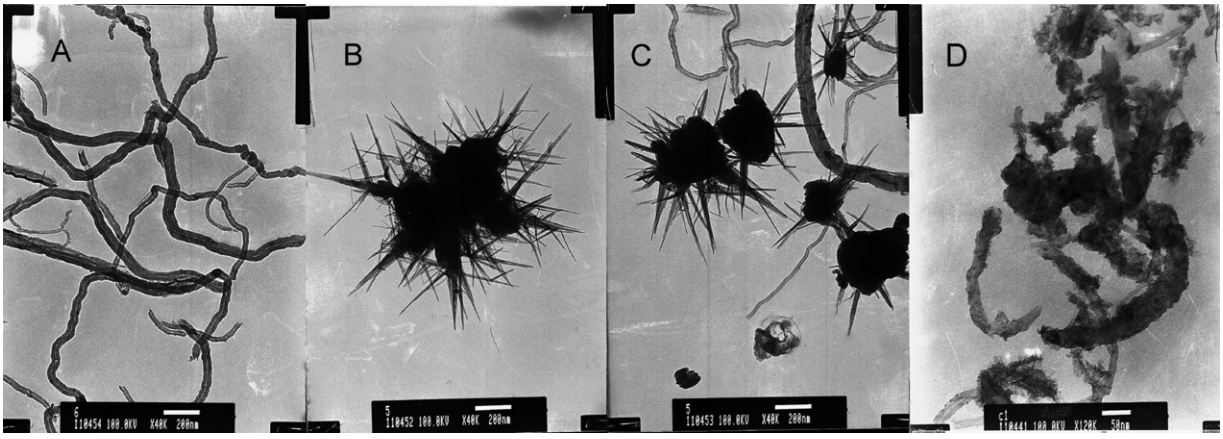

Fig. 2. TEM images of (A) pure CNTs, (B) pure MnO_2, (C) mechanically mixed MnO_2/CNTs and (D) in situ MnO_2/CNTs.

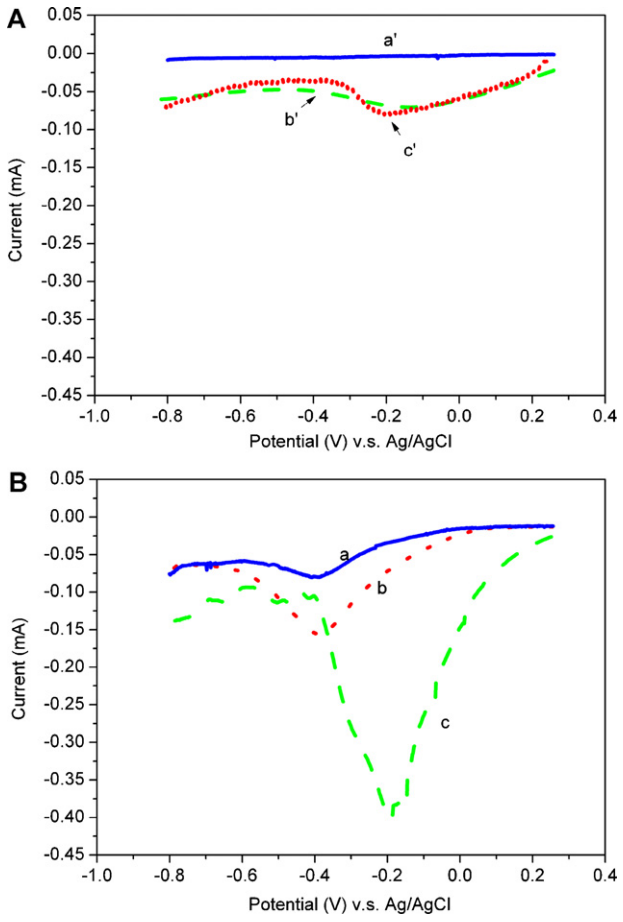

Fig. 3. LSV curves obtained in the PBS medium saturated by N_2 (A) and O_2 (B) for the bare CNTs(a′, a), the mechanically mixed MnO_2/CNTs(b′, b), and the in situ MnO_2/CNTs (c′, c). Scan rate: 20 mV s^{-1}.

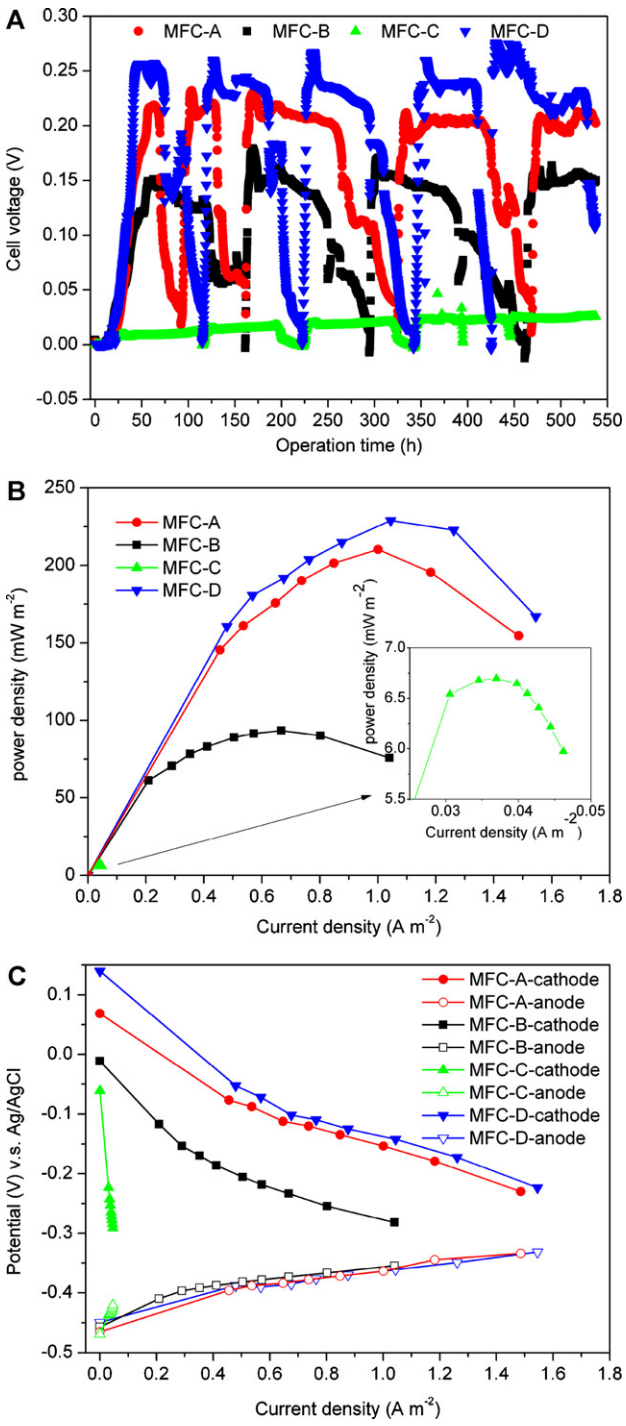

Fig. 4. Performance of MFC equipped with the in situ MnO_2/CNTs (MFC-A), the mechanically mixed MnO_2/CNTs (MFC-B), the bare CNTs (MFC-B) and the Pt/C cathode (MFC-D): (A) voltage production as a function of time, (B) power density, and (C) anode and cathode polarization curves.

was much greater than that of the mechanically mixed MnO_2/CNTs (−0.16 mA) and bare CNTs (−0.08 mA). This suggests an effective decomposition of the electrogenerated hydrogen peroxide by the in situ MnO_2/CNTs [25]. In contrast to conventional carbon-supported electrocatalysts, the higher catalytic activity of the in situ MnO_2/CNTs was attributed to the outstanding electrical properties of the CNTs. More importantly, the improved dispersion of MnO_2 over the surfaces of the CNTs (as revealed by the TEM) favors oxygen adsorption on the surfaces of the in situ MnO_2/CNTs, facilitating electron transfer through the films and decreasing the ORR overpotential. In addition, the presence of oxygenated groups on the surface of the CNTs, partially due to oxidation by permanganate, may facilitate oxygen reduction, as reported by Kinoshita [38]. For the mechanically mixed MnO_2/CNTs, the mixing homogeneity of MnO_2 with the CNTs was poor, resulting in relatively low conductivity and weaker ORR performance. Thus, it was expected that among the three samples, the in situ MnO_2/CNTs would constitute the most effective cathode catalyst material for MFCs.

3.3. MFC performance

The performance of MFCs with the in situ MnO_2/CNTs (MFC-A) and the mechanically mixed MnO_2/CNTs (MFC-B) was evaluated alongside that of the bare CNTs (MFC-C) and the Pt/C (MFC-D) cathodes by monitoring cell voltage output, anode and cathode polarization, and power density. As shown in Fig. 4A, MFC-A delivered a maximum stable voltage of 0.22 V, which was larger than that achieved with MFC-B (0.16 V) and MFC-C (0.02 V), but lower than that achieved with MFC-D (0.26 V). The power density versus current density curves are presented in Fig. 4B. The maximum power density of 210 mW m^{-2} produced by MFC-A was higher than from the densities produced by MFC-B (93 mW m^{-2}) and MFC-C (8 mW m^{-2}) and comparable with the density produced by MFC-D (229 mW m^{-2}). The low power generation of MFC-B and MFC-C could be explained by their higher internal resistances (R_{in}, listed in Table 1). The differences of R_{in} among these MFCs may have been due to the electrical characteristics of the various catalysts, particu-

Table 1
Performance of MFC based on different cathodic catalysts. R_{ct}: charge-transfer resistance.

Catalyst	OCP *vs.* Ag/AgCl (mV)	Internal resistance (Ω)	Cathode R_{ct} (Ω)	Maximum power density (mW m^{-2})
CNTs	0.40	7683.9	4200	8
Mechanically-mixed MnO_2/CNTs	0.44	358.7	50	93
In-situ MnO_2/CNTs	0.53	293.9	35	210
Pt/C	0.58	294.8	20	229

larly conductivity [24]. Therefore, the sufficient dispersion of MnO_2 over the surfaces of the CNTs resulted in a high conductivity and decreased the cathodic resistance of the in situ MnO_2/CNTs, thus achieving a better performance in MFC-A.

It was evident from the anode and cathode polarization curves (Fig. 4C) that the cathode was the limiting factor in these MFC reactors. For instance, in MFC-A, with increased current densities of 0–1.5 Am^{-2}, the anode potential increased insignificantly from −0.47 to −0.33 V, whereas the cathode potential dropped from 0.07 to −0.23 V. The larger driving force with an overpotential of 0.30 V required for the cathode compared to the value of 0.14 V required for the anode indicates that power generation from the MFC was dominated by cathode polarization. In the case of the bare CNTs cathode, the more rapid decrease in cathodic potential from the open circuit potential (OCP) suggests poor reaction kinetics. The high activation energy of the ORR can explains the high cathodic overpotential observed with the bare CNTs cathode. The in situ MnO_2/CNTs lowered the cathodic overpotential compared with the bare CNTs and mechanically mixed MnO_2/CNTs, suggesting a decrease of activation energy needed for ORR. Moreover, although the cathode OCP of the in situ MnO_2/CNTs is approximately 0.07 V, which is more negative than that of Pt/C, its overpotential was comparable to that observed with the Pt/C cathode. The electrochemical reaction rates in a fuel cell can also be evaluated by its OCP. A higher OCP value is related to a higher reaction rate [39]. The OCP of the MFC-A was 0.53 V, which was a little lower than that of MFC-D (0.58 V) but much higher than that of others (Table 1). These results indicate an enhanced ORR performance due to the in situ MnO_2/CNTs, which is consistent with the LSV test.

EIS tests were performed to investigate the cathode resistances of the MFCs. Here, the charge-transfer resistance (R_{ct}) is indicated by the diameter of the first semicircle in the Nyquist curve [40]. As shown in Fig. 5, the R_{ct} of the MFC-A was approximately 35 Ω, whereas that of the MFC-B was approximately 50 Ω, and both are higher than that of MFC-D (20 Ω). It is well known that the electrochemical reaction rate is inversely proportional to the R_{ct}

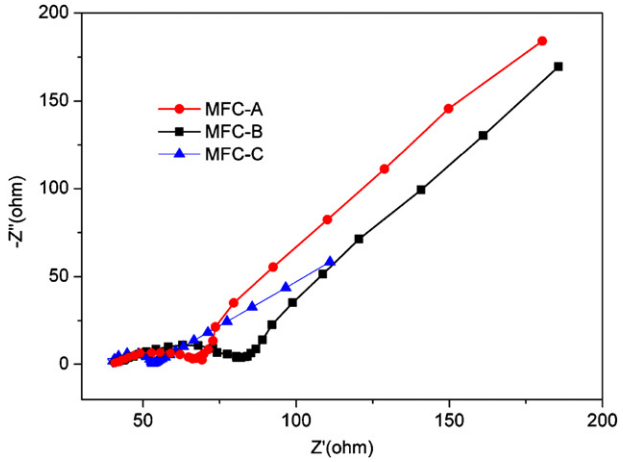

Fig. 5. Nyquist curves of EIS test for the MFC equipped with the In-situ MnO_2/CNTs (MFC-A), the mechanically mixed MnO_2/CNTs (MFC-B) and the Pt/C cathode (MFC-D).

[40]. The improvement in R_{ct} suggests that the in situ MnO_2/CNTs enhanced the ORR rate compared with the mechanically mixed MnO_2/CNTs. The higher electron-transfer efficiency likely resulted from the improved catalyst surface area available for ORR and the enhanced conductivity of the in situ MnO_2/CNTs (due to the three-dimensional network structure). Therefore, the above results strongly suggest that the in situ MnO_2/CNTs are a good alternative to Pt/C for an MFC cathode.

MnO_x has previously been used as a cost-effective electrocatalyst for ORR in MFCs [22–25]. In comparison with a prior work [25] that also used MnO_x as an ORR electrocatalyst, where the MnO_x was prepared by an electrochemical deposition method but without a catalyst support, the in situ MnO_2/CNTs using CNTs as a catalyst support delivered 2.29 times higher power output (2544 *vs.* 773 mW m^{-3}). It is well known the poor conductivity of the MnO_x is a major problem for its efficient use in electrochemical applications [28]. MnO_x can be incorporated into electronically conductive materials to improve its electrochemical performance, which is crucial for enhancing ORR in an MFC cathode. Therefore, the improvement of in situ MnO_2/CNTs catalyzed-MFC was due to the use of highly conductive CNTs as a support material. The three-dimensional network structure of this hybrid catalyst, wherein the MnO_2 crystals are intertwined with highly conductive CNTs, greatly increased its active surface, and electrons transport to the electrode was facilitated by the conductivity paths provided by CNTs. Further studies are required to understand the mechanisms of the ORR on the in situ MnO_2/CNTs nanostructures in more detail and to optimize the performance of the system.

4. Conclusions

Manganese dioxide was chemically coated onto CNTs by a simple in situ hydrothermal method to form in situ MnO_2/CNTs, which were investigated as an efficient catalyst for the ORR in an MFC. Due to the sufficient and uniform dispersion of MnO_2 over the surfaces of the CNTs, an electrode based on the in situ MnO_2/CNTs exhibited improved electrocatalytic activity for the ORR in a neutral-pH medium compared with mechanically mixed MnO_2/CNTs. Furthermore, the maximum power density of 210 mW m^{-2} produced by an MFC with the in situ MnO_2/CNTs was 2.3 times of that produced by an MFC using the mechanically mixed MnO_2/CNTs (93 mW m^{-2}) and comparable with that generated by an MFC with a Pt/C (229 mW m^{-2}). The results demonstrate that CNTs are an ideal catalyst support material for MnO_2 and that in situ MnO_2/CNTs are a good alternative to Pt/C in practical MFC applications.

Acknowledgement

The authors gratefully acknowledge the financial support provided by the National Natural Science Fund of China (No. 20977032).

References

[1] D. Lovley, Nat. Rev. Microbiol. 4 (2006) 497–508.
[2] B.E. Logan, Nat. Rev. Microbiol. 7 (2009) 375–381.
[3] S. Cheng, H. Liu, B.E. Logan, Electrochem. Commun. 8 (2006) 489–494.
[4] Y. Qiao, S. Bao, C. Li, Energy 3 (2010) 544–553.

[5] H. Rismani-Yazdi, S.M. Carver, A.D. Christy, O.H. Tuovinen, J. Power Sources 180 (2008) 683–694.
[6] F. Harnisch, S. Wirth, U. Schröder, Electrochem. Commun. 11 (2009) 2253–2256.
[7] J.M. Morris, S. Jin, J.Q. Wang, C.Z. Zhu, M.A. Urynowicz, Electrochem. Commun. 9 (2007) 1730–1734.
[8] E. HaoYu, S. Cheng, K. Scott, B. Logan, J. Power Sources 171 (2007) 275–281.
[9] F. Zhao, F. Harnisch, U. Schroder, F. Scholz, P. Bogdanoff, I. Herrmann, Electrochem. Commun. 7 (2005) 1405–1410.
[10] Y. Yuan, S.G. Zhou, L. Zhuang, J. Power Sources 195 (2010) 3490–3493.
[11] L. Birry, P. Mehta, F. Jaouen, J.P. Dodelet, S.R. Guiot, B. Tartakovsky, Electrochim. Acta 56 (2011) 1505–1511.
[12] Y. Yuan, J. Ahmed, S. Kim, J. Power Sources 196 (2011) 1103–1106.
[13] L. Deng, M. Zhou, C. Liu, L. Liu, C. Liu, S. Dong, Talanta 81 (2010) 444–448.
[14] L. Wang, P. Liang, J. Zhang, X. Huang, Bioresour. Technol. 102 (2011) 5093–5097.
[15] L. Fu, S.-J. You, G.-Q. Zhang, F.-L. Yang, X.-H. Fang, Z. Gong, Biosens. Bioelectron. 26 (2011) 1975–1979.
[16] J.R. Kim, J.-Y. Kim, S.-B. Han, K.-W. Park, G.D. Saratale, S.-E. Oh, Bioresour. Technol. 102 (2011) 342–347.
[17] A. ter Heijne, H.V.M. Hamelers, C.J.N. Buisman, Environ. Sci. Technol. 41 (2007) 4130–4134.
[18] K. Gong, P. Yu, L. Su, S. Xiong, L. Mao, J. Phys. Chem. C 111 (2007) 1882–1887.
[19] F. Cheng, J. Shen, W. Ji, Z. Tao, J. Chen, ACS Appl. Mater. Interfaces 1 (2009) 460–466.
[20] P. Clauwaert, D. Van der Ha, N. Boon, K. Verbeken, M. Verhaege, K. Rabaey, W. Verstraete, Environ. Sci. Technol. 41 (2007) 7564–7569.
[21] I. Roche, K. Scott, J. Electroanal. Chem. 638 (2010) 280–286.
[22] L. Zhang, C. Liu, L. Zhuang, W. Li, S. Zhou, J. Zhang, Biosens. Bioelectron. 24 (2009) 2825–2829.
[23] I. Roche, K. Katuri, K. Scott, J. Appl. Electrochem. 40 (2010) 13–21.
[24] X. Li, B. Hu, S. Suib, Y. Lei, B. Li, J. Power Sources 195 (2010) 2586–2591.
[25] X.-W. Liu, X.-F. Sun, Y.-X. Huang, G.-P. Sheng, K. Zhou, R.J. Zeng, F. Dong, S.-G. Wang, A.-W. Xu, Z.-H. Tong, H.-Q. Yu, Water Res. 44 (2010) 5298–5305.
[26] C.W.B. Bezerra, L. Zhang, H. Liu, K. Lee, A.L.B. Marques, E.P. Marques, H. Wang, J. Zhang, J. Power Sources 173 (2007) 891–908.
[27] K. Lee, L. Zhang, H. Lui, R. Hui, Z. Shi, J. Zhang, Electrochim. Acta 54 (2009) 4704–4711.
[28] Y. Hou, Y. Cheng, T. Hobson, J. Liu, Nano Lett. 10 (2010) 2727–2733.
[29] N. Jha, A. Leela Mohana Reddy, M. Shaijumon, N. Rajalakshmi, S. Ramaprabhu, Int. J. Hydrogen Energy 33 (2008) 427–433.
[30] S. Ramaprabhu, A. Reddy, Int. J. Hydrogen Energy 32 (2007), 4772–4278.
[31] S. Takenaka, T. Iguchi, E. Tanabe, H. Matsune, M. Kishida, Carbon 47 (2009) 1251–1257.
[32] A.L.M. Reddy, M.M. Shaijumon, S.R. Gowda, P.M. Ajayan, Nano Lett. 9 (2009) 1002–1006.
[33] F. Teng, S. Santhanagopalan, D.D. Meng, Solid State Sci. (2010).
[34] S. Liang, F. Teng, G. Bulgan, R. Zong, Y. Zhu, J. Phys. Chem. C 112 (2008) 5307–5315.
[35] H. Liu, B.E. Logan, Environ. Sci. Technol. 38 (2004) 4040–4046.
[36] J. Sun, Y.Y. Hu, Z. Bi, Y.Q. Cao, J. Power Sources 187 (2009) 471–479.
[37] C. Yuan, L. Su, B. Gao, X. Zhang, Electrochim. Acta 53 (2008) 7039–7047.
[38] K. Kinoshita, Electrochemical Oxygen Technology, Wiley-Interscience, New York, 1992.
[39] B.E. Logan, B. Hamelers, R.A. Rozendal, U. Schrorder, J. Keller, S. Freguia, P. Aelterman, W. Verstraete, K. Rabaey, Environ. Sci. Technol. 40 (2006) 5181–5192.
[40] Z. He, F. Mansfeld, Energy Environ. Sci. 2 (2009) 215–219.